Repositorio Institucional de la Universidad Autónoma de Madrid

https://repositorio.uam.es

Esta es la **versión de autor** del artículo publicado en:
This is an **author produced version** of a paper published in:

Advanced Energy Materials 8.25 (2018): 1800681

DOI: https://doi.org/10.1002/aenm.201800681

Copyright: © 2018 Wiley‐VCH Verlag GmbH & Co. KGaA, Weinheim

El acceso a la versión del editor puede requerir la suscripción del recurso

Access to the published version may require subscription

WILEY-VCH

DOI: 10.1002/ (manuscript number)
Article type: Full Paper

Title: Tetrathienoanthracene and Tetrathienylbenzene Derivatives as Hole-Transporting Materials for Perovskite Solar Cell

*Author(s), and Corresponding Author(s)**

Diana Elizabeth Meza Rojas, Kyung Taek Cho, Yi Zhang, Maxence Urbani, Nouar Tabet, Gema de la Torre, Mohammad Khaja Nazeeruddin,* Tomás Torres **

Dr. D. E. Meza Rojas, Dr. M. Urbani, Dr. G. de la Torre, Prof. T. Torres
Departamento de Química Orgánica, Universidad Autónoma de Madrid, Cantoblanco, 28049 Madrid, Spain.
E-mail: gema.delatorre@uam.es, tomas.torres@uam.es

K. T. Cho, Dr. Y. Zhang, Dr. M. Urbani, Prof. M. K. Nazeeruddin
Group for Molecular Engineering of Functional Materials, Institute of Chemical Sciences and Engineering, EPFL, Valais Wallis, Rue de l'Industrie 17, 1950 Sion, Switzerland.
E-mail: mdkhaja.nazeeruddin@epfl.ch

Dr. M. Urbani, Prof. T. Torres
IMDEA-Nanociencia, Campus de Cantoblanco, 28049 Madrid, Spain.

Dr. G. de la Torre, Prof. T. Torres
Institute for Advanced Research in Chemical Sciences (IAdChem), Universidad Autónoma de Madrid, 28049 Madrid, Spain.
Prof. Nouar Tabet, Qatar Environment and Energy Research Institute, Hamad Bin Khalifa University (HBKU), Qatar Foundation, Doha, 5825, Qatar

Keywords: solar energy conversion – perovskite solar cells – hole-transporting materials – tetrathienoanthracenes – tetrathienylbenzenes

Abstract

The synthesis and characterization of two related families of star-shaped thiophene-containing hole transporting materials (HTMs) based on fused tetrathienoanthracene and non-fused tetrathienylbenzene cores are reported. All of them are endowed with four terminal (4,4'-dimethoxy)diphenylamino groups that are linked either directly to the core or shows a different type of bridges (*i.e.,* thiophene-phenyl or phenyl rings). The novel HTMs are tested in mixed-ion perovskite ($Cs_{0.1}FA_{0.74}MA_{0.13}PbI_{2.48}Br_{0.39}$) solar cells, and power conversion

efficiencies (PCE) of up to 18.8% are measured under 1 sun irradiation, comparable with the efficiency obtained for the reference cell using *Spiro*-OMeTAD as a HTM.

1. Introduction

Photovoltaic (PV) devices, which directly convert solar energy to electrical energy, are powerful, environmentally clean, renewable sources. In particular, perovskite solar cells (PSCs) have become one of the most promising and low-cost technologies to replace the traditional energy sources.[1–8] The organic–inorganic perovskites have an ABX_3 structure and are typically comprised of an organic cation (where A = methylammonium (MA^+), formamidinium (FA^+) and/or Cs^+), a divalent metal (where B = Pb^{2+}, Sn^{2+}, or Ge^{2+}), and an anion (where X = Cl^- Br^-, and/or I^-).[4] They exhibit some of the properties of an ideal photoactive material, such as good light-harvesting capability over the visible to the near-infrared solar spectrum and tuneable band gap, [9] relatively low exciton binding energy,[10] high charge carrier mobilities with long diffusion lengths and ambipolar behaviour.[11,12]

The optoelectronic properties of perovskite materials can be easily and widely tuned by modifying anionic and/or cationic components.[9, 13] However, pure ABX_3 perovskite compounds, such as $MAPbX_3$, $FAPbX_3$ and $CsPbX_3$ (with X = Br or I) present also some shortcomings for photovoltaic applications, in particular non-ideal band gap,[14] poor stability under continuous light and high temperature-exposure[15,16] and low chemical stability[17] under ambient atmosphere (oxygen[18] and moisture induced degradations). In this regard, "mixed perovskites", which are composed of mixed cations (MA^+, FA^+ and/or Cs^+) and halides (Br^- and/or I^-), have emerged as efficient and thermally more stable materials for photovoltaic applications.[19,20] Moreover, to date, the best PSC efficiencies have been obtained with mixed perovskites, such as double mixed-halide $MAPbBr_xI_{(3-x)}$,[21] double mixed-cation $FA_xMA_{(1-x)}PbI_3$,[22] or more recently, triple-cation (MA^+, FA^+ and Cs^+), dual-halide (Br^- and I^-) mixed-perovskites with the generic form of $Cs_x(MA_{0.17}FA_{0.83})_{(1-}$

$_{x)}Pb(I_{0.83}Br_{0.17})_3$[23–26] that achieved efficiencies higher than 21%.[23,24] Other approaches have been also envisaged in the recent years to improve the stability and/or efficiency of PSCs, as for instance by 2D/3D interface engineering of the perovskite [27] or introducing ferroelectric properties to obtain a bulk photovoltaic effect (BPVE). [28–33]

PSCs are typically composed of multiple inter-stacked layers, namely, a transparent electrode, an electron transporting layer (ETL), a perovskite photoactive material, a hole-transporting layer (HTL), and a metal counter electrode. In the case of planar heterojunction PSCs, where the ETL and HTL are implemented as monolayers, the performance is strongly affected by the charge transporting layers in general, and by HTLs in particular. 2,2′,7,7′-tetrakis(*N*,*N*′-di-*p*-methoxyphenylamine)-9,9′-spirobifluorene (*Spiro*-OMeTAD) is frequently utilized as hole-transporting material (HTM) in PSCs with conventional structures. As a result, high performance devices are achieved, although cobalt (III) complex doping of the HTL is necessary to achieve good mobility.[34] Unfortunately, *Spiro*-OMeTAD presents some drawbacks, such as its low stability under heat and light socking conditions, and its complicated synthesis, and purification, which make it unsuitable for realistic applications. Therefore, for commercial purposes, the exploration of alternative HTMs with high performance and cost-effectiveness is required. In this regard, various kinds of small molecule and polymeric HTMs have been developed and reported as potential alternatives to *Spiro*-OMeTAD.[35] Especially, small molecule HTMs have been widely developed because they are relatively cheap and easy to purify. These molecules consist of an aromatic core decorated with diarylamines, triarylamines[36 - 38] and/or carbazole[39] derivatives in a star-shape configuration. A range of aromatic cores with extended π-conjugated structures arises from the organic photovoltaic field, which also relies on the use of p-type semiconductors.[35] In particular, thiophene-based derivatives have been widely investigated as organic semiconducting materials due to their optoelectronic properties and high hole mobilities. These features have encouraged many scientists to design and synthesize molecules

comprising thiophene–based central cores, and further test them as HTLs in PSCs. Therefore, various types of small molecule HTMs based on thiophene,[40] 3,4-ethylenedioxythiophene,[41–43] benzodithiophene,[44] benzotrithiophene,[45] silolothiophene,[46] spirothiophene,[47] fluorine-dithiophene,[48] and, more recently, tetrathienoanthracene[49] have been implemented in different PSC architectures, reaching efficiencies as high as 20.2%.[48] Moreover, it has been recently established that the presence of thiophene enables the sulphur–iodine interaction with the perovskite layer, which promotes a more efficient hole extraction. Here, we report the design, synthesis, characterization and photovoltaic performance in mixed perovskite solar cells of two families of star-shaped thiophene-containing HTMs based on tetrathienoanthracene (**TTA1**–**3**) and tetrathienylbenzene cores (**TTB1**–**3**), all of them endowed with four terminal (4,4'-dimethoxy)diphenylamino groups (**Figure 1**). The two families of compounds present either a direct bond between the diphenylamino moieties to the core (**TTA1** and **TTB1**), or different type of bridges, namely phenyl (**TTA2** and **TTB2**) and thiophene-phenyl (**TTA3** and **TTB3**), between the central core and the terminal diphenylamino substituents. The motivation of this work is to modulate both the HOMO level of the molecules (to find a good match with the valence band edge of the perovskite) and the crystallinity of the films prepared with these molecules, as a function of the electronic character of the substituents and the planarity and rigidity of the molecules. It is important to mention that one of the **TTA** derivatives, namely **TTA2**, has been recently prepared and implemented in PSCs by the groups of N. Martin and M. K. Nazeeruddin.[49] The PSCs prepared with this derivative showed a maximum PCE of 18.1%. Therefore, we have tested the capabilities of these two families of HTMs, **TTA***n,* and **TTB***n*, in mixed PSCs. In particular, we have used a triple-cation (Cs^+, FA^+, and MA^+) dual-halide (Br^- and I^-) mixed-perovskite as a photoactive material with nominal formula $Cs_{0.1}FA_{0.74}MA_{0.13}PbI_{2.48}Br_{0.39}$. Advantages of this perovskite are: i) its thermal stability; ii) low degree of impurities; iii) improved and stabilized efficiencies;[23-26] and iv) low dependence to variations during the

fabrication process (solution proceeded), such as temperature, solvent vapours or heating protocols, hence affording more reproducible device performances.[23]

We systematically observed that the PSC devices fabricated with the non-fused **TTB***n* HTMs gave significantly poor performances in comparison with their corresponding fused **TTA***n* analogues, which can be rationalized in terms of better hole-transporting properties and intermolecular ordering due to the extended π-conjugated structures of the **TTA** aromatic core that enables stacking of their planar structure through intramolecular π–π interactions. Remarkably, **TTA3** endowed with a phenyl-thiophene linker between the **TTA** core and (4,4'-dimethoxy)diphenylamino moieties reached the highest efficiencies of the series, up to 18.8%, in mixed perovskite solar cells, comparable to those of the reference devices made with the standard HTM *Spiro*-OMeTAD under the same experimental conditions.

2. Results and Discussion

2.1. Synthesis

The synthetic routes for the preparation of **TTB1**–**3** and **TTA1**–**3** are shown in **Scheme 1**. The detailed synthetic procedures and characterization data are given in the Supporting Information. All the compounds were prepared using a common precursor, the brominated tetrathienylbenzene core **1**, which was prepared following reported procedures involving a 4-fold Stille coupling of 1,2,4,5-tetrabomobenzene with 2-(tributylstannyl)thiophene, followed by a bromination with *N*-bromosuccinimide.[50] From this compound, the tetrabrominated **TTA** core **2** was easily prepared by oxidative cyclization with $FeCl_3$.[50] Finally, the different *p*-alkoxyarylamine precursors (**3**–**5**), which were either commercially available or prepared following reported procedures,[51,52] were covalently linked to the central cores **1** and **2** by Pd-catalyzed cross-coupling methodologies. Specifically, Buchwald-Hartwig coupling was applied for the synthesis of **TTB1** and **TTA1**, Suzuki coupling for the synthesis of **TTB2** and

TTA2, and Stille coupling for **TTB3** and **TTA3** derivatives. The yields in the cross-coupling reaction range from 32% to 85%, but most of them are from moderate to high, considering that all chemical conversions from **1/2** in the respective target compounds implied a fourfold cross-coupling. Overall yields starting from commercially available materials series range from 26% to 41%, for the **TTB** series, and from 22% to 58% for the **TTA** derivatives.

It is worth mentioning that, although the **TTB** are the immediate synthetic precursors of their **TTA** counterparts, direct conversion of **TTB1–3** in their **TTA1–3** counterparts are not realistic since other aromatic units can be also involved in oxidative cyclizations. The only transformation that we attempted was the conversion of **TTB1** in **TTA1** and, indeed, we obtained a complex mixture of compounds. The molecular structure of the new HTMs was confirmed by ^{1}H, ^{13}C, APT, DEPT-135 and HMQC NMR spectroscopy and MALDI-TOF mass spectrometry (see the Supporting Information). The compounds have good solubility in most of the common organic solvents.

Importantly, we have evaluated the costs for the preparation of 1g of **TTA3** in comparison with the costs reported by Petrus *et al* for the synthesis of *Spiro*-OMeTAD (see the Supporting Information). [53] For **TTA3**, we have estimated that the cost is 43–44 \$ g^{-1}, which means that it is 2.4 times lower compared to that of *Spiro*-OMeTAD (92 \$ to 108 \$ g^{-1}). Thermal stability of **TTA3** has been tested by TGA analysis, showing degradation of the molecule well above 400ºC (see the Supporting Information).

2.2. Optical and electrochemical properties

The optical properties of **TTB1–3** and **TTA1–3** HTMs were studied using absorption (**Figure 2a** and **2d**) and emission (**Figure 2b** and **2e**) spectroscopy in chloroform solution, and the results are summarized in **Table 1**. For the **TTB***n* series, absorption peaks centred in the range 385–418 nm are observed (Figure 2a). In particular, the absorption of **TTB3** is quite red-shifted as compared to the other members of the series, which can be attributed to an increase

in π–conjugation due to the planarity imposed by the thiophene-thiophene bond. The emission spectra were registered after excitation at a maximum wavelength of absorption, and exhibit maxima centred between 521 nm and 541 nm (Figure 2b). The large Stokes shift for all the compounds (~130 nm) is indicative of significant differences in the structure and dipolar moments between the excited and ground states. From the intersection of emission and absorption spectra, we could obtain the zero–zero excitation energy (E_{0-0}) and, therefore, the optical band gap (Table 1). In the case of the **TTA*n*** series, absorption bands appear in the spectral region between 400–460 nm (Figure 2d). In general, all the transitions present higher molar absorptivity than those of the **TTB*n*** compounds. Also in this series, a bathochromic shift of ~55 nm is observed in the π–π* transition of **TTA3** with respect to **TTA-1**,**2** (see Table 1 and Figure 2d), which is also attributed to the more planar configuration of **TTA3**. It should be noted that in the case of the **TTA1** molecule, although the λ of its maximum and sharp absorption matches those of **TTA2**, two low-intense, bathochromically shifted transitions arise in the spectrum of **TTA1**, instead of the broad decay towards the red displayed by the other members of the series (Figure 2d). On the other hand, in the case of **TTA2**, a broad, low-intense band at *ca*. 600 nm is discernible. To investigate a possible charge-transfer origin of the latter transition, we have performed solvent-dependent studies (see Supporting Information). However, no dependence on the solvent polarity was found. Additionally, no intensity changes were observed at different concentrations, indicating that aggregation does account for the development of this band. Further photophysical studies would be necessary to elucidate unequivocally the nature of this transition, but this is not the scope of the present work.

Emission spectra (Figure 2e) show that all **TTA** molecules render relatively large Stokes shifts, but smaller than the ones exhibited by **TTB** compounds, which is consistent with the more rigid structure of the **TTA** core. The optical bandgap was estimated from the

intersection of the corresponding normalized absorbance and emission spectra. The $E_{0\text{-}0}$ values obtained are rather similar to those of the **TTB** series (Table 1).

To take a full picture of the electronic features of the **TTB***n* and **TTA***n* derivatives, we also performed CV measurements. Cyclic voltamograms are shown in **Figure 2c** and **2f**. Well-resolved oxidization is observed for **TTB2** and **TTB3**, which are ascribed to the removal of electrons from the triphenylamine units.[54] However, a poorly resolved, non-reversible oxidation appears in the CV of **TTB1**. The first oxidation peaks observed for the **TTA***n* derivatives are, in all cases, non-reversible processes. The voltamogram of **TTA3** displays additional oxidations, assigned to the formation of stable radical cations and di-cations delocalized over the conjugated backbone. The HOMO energy levels were calculated from the CV data (Table 1), by using the equation $E_{HOMO} = -(E_{[onset,\ ox\ vs.\ Fc/Fc+]} + 5.1)$ (eV).[55] As none of the compounds show reduction peaks in the electrochemical window of our experiments, the LUMO energies were estimated by subtracting the $E_{0\text{–}0}$ values from the electrochemically determined HOMO energies. We are aware that this practice for the calculation of LUMO energies is not fully accurate [56] but it is commonly extended for the evaluation of the HOMO/LUMO levels of organic molecules when it comes to assess their photovoltaic potential. **Figure 3** depicts the calculated HOMO/LUMO values for HTMs **TTB***n* and **TTA***n* derivatives and *Spiro*-OMeTAD, in comparison with the conduction and valence band of mixed-perovskite and TiO_2, and the Fermi level of the gold counter-electrode. The HOMO level of our new HTMs are comparable to that of *Spiro*-OMeTAD (–5.16 eV,[49] –5.22 eV[57,58]), except that of **TTB1**, which lies significantly lower (–5.48 eV). Overall, the HOMO energy level of all of our new HTMs are well aligned with the valence band (VB) edge of the mixed-ion perovskite used in this study (assumed to be at –5.72 eV),[26] which would facilitate the extraction of the holes from the perovskite layer in the device. Moreover, the large barrier between the conduction band (CB) of the perovskite and LUMO of the

HTMs could block the electrons efficiently and thus reduce the recombination process at perovskite/HTM interface.

The new small molecules **TTA*n*** and **TTB*n*** were tested as HTM in solution-processed PSC devices. The photoactive material used in this study is a triple-cation (Cs^+, FA^+, and MA^+) dual-halide (Br^-, I^-) mixed- perovskite as light absorber with the nominal formula $Cs_{0.1}FA_{0.74}MA_{0.13}PbI_{2.48}Br_{0.39}$. The HTM layer was applied by spin-coating solutions of **TTA*n*** or **TTB*n*** (10–50 mM) in either 1,1,2,2-tetrachloroethane (TCE) or chlorobenzene (PhCl) and containing cobalt dopant (FK209; 5 mol%), Li-TFSI (50 mol%), and *tert*-butylpyridine (330–340 mol%) as additives. The detailed procedure for the fabrication of the solar cells is given in the Experimental Section.

Except for **TTA2**, much better performances and reproducibility were systematically obtained for devices fabricated with HTMs spin-coated from TCE solutions instead of PhCl (**Table 2** and **Table S1** in Supporting Information). Only **TTA2** gave significantly better efficiencies when spin-coated from PhCl (PCE = 14.09%) instead of TCE solutions (PCE = 9.69%), which is in agreement with the conditions previously reported for this compound in PSC.[49] Since the homogeneity of the films, which depends strongly on the solvent, solubility and, above all, chemical structure of the molecule- is closely related to the morphology, and hence to the conducting behaviour of the HTM inside the device, we anticipate that this is a crucial factor that explains most likely the observed differences in performance and reproducibility of these devices within this series of compounds (*vide infra*).

In the **TTA*n*** series, the short-circuit current density (J_{SC}) values were constantly high (above 20 mA/cm^2), which witnesses the excellent hole-transporting properties of the **TTA** core. This is in agreement with the estimated HOMO energy level of the HTMs (–5.27, –5.23 and –5.20 eV for **TTA1**, **TTA2** and **TTA3**, respectively) that lies very close to that of *Spiro*-OMeTAD (–5.22 eV)[57] and well-aligned with the valence band (VB) edge of our mixed-perovskite (assumed to be at –5.72 eV).[26] Thus, we discard any significant difference concerning the

driving force for charge extraction for this series of compounds. Instead, the main difference between these three HTMs comes from the FF values. **TTA2** cells display low FF when prepared both from TCE and PhCl solutions (*ca.* 60–62%), compared to **TTA1** and **TTA3** cells (*ca.* 80% and 73% in TCE, respectively). Unfortunately, we cannot explain why **TTA2** cells systematically gave lower values that those previously reported.[49] It is worth to note that **TTA1** and **TTA3** systematically lead to excellent fill factor values (FF > 70–75%), comparable (**TTA3**) and even superior (**TTA1**) than those obtained for *Spiro*-OMeTAD. As commented above, the formation of homogenous films with good morphology and conductivity should explain most likely the observed differences in performance (especially the *F.F* values), and hence efficiency, between the three HTMs. Notably, **TTA3**/PSC devices reached larger open-circuit voltages (V_{OC}) than all other devices, including that of the reference cell made with *Spiro*-OMeTAD. Impressive V_{OC} values, with a maximum of up to 1.15V, were obtained with this HTM.

A typical *J-V* curve measured under forward and reverse bias for a PSC cell made with HTM **TTA3** is depicted on **Figure 5A**. A scan rate of 10 mV s^{-1} has been applied in order to minimize the hysteresis effects stemming from the perovskite material and, as it can be seen in the figure, there is almost no hysteresis when tested under the described conditions. The EQE spectrum recorded for **TTA3**/PSC (**Figure 5B**) shows good values (> 82%) in the whole UV-Vis and near-IR regions. The integrated $\boldsymbol{J_{SC}}$ value calculated from the EQE spectrum (20.71 mA/cm^2) matches well those typically obtained from *J-V* curves recorded for **TTA3**/PSC devices (*ca.* 21 mA/cm^2).

Turning to the **TTB***n* series, it is clear that the J_{SC} values were consistently much lower by a factor of 2-to-5 with respect to their **TTA***n* analogues, with values below 5–11 mA/cm^2. Since the HOMO energy level of this series of HTMs (except **TTB1**) are very similar to that of their **TTA***n* analogues, and considering that the substituents are the same, the influence of the stacking of the molecules within the film seems to be critical on the short-circuit (J_{SC}) values.

This emphasizes that the fused and large aromatic core of **TTA** powers excellent hole-transporting properties of the **TTA***n* films due to an appropriate stacking of the molecules, which is not the case for **TTB***n*s. In addition, the V_{OC} of **TTA1**/PSC is significantly lower (*ca.* 0.8 V) compared to all other cells (*ca.* 1.0V - 1.1V). Finally, it is important to point out that the photovoltaic performances of the **TTA***n*-based devices gradually and slightly improved over time, and in fact, optimal performances were most often obtained one month after cell assembly (see Figures S39–S41 and Table S2–4 in the Supporting Information). Moreover, TGA analysis of our champion HTM **TTA3** indicates thermal stability of this compound at temperature up to 400ºC (see Figure S32 in the Supporting Information). These preliminary results are therefore promising to target stable perovskite cells made with this new HTM, and stability test under light-soaking and thermal stress will be foreseen in the future.

3. Conclusion

We have synthesized two classes of HTMs containing either tetrathienoanthracene or tetrathienylbenzene cores, both series of compounds being functionalized with four diphenylamino groups that are linked either directly or through different type of bridges to the central core. The HOMO level of the new HTMs are comparable to that of *Spiro*-OMeTAD, and are well aligned with that of mixed-perovskite valence band, which facilitates the extraction of the holes from the perovskite layer in the device. The performance characteristics of tetrathienoanthracene-based HTMs (**TTA1-TTA3**) are superior to those of the tetrathienylbenzene-containing derivatives (**TTB1-TTB3**). We reckon that the excellent performance of **TTA***n* HTMs is due to the stacking of molecules in the film, resulting in better hole mobility compared to the **TTB***n* series. Also, the increased absorption in the visible range of **TTA***n* HTMs with regard to the **TTB***n* series (and also the *Spiro*-OMeTAD reference) could have a role on the performance of **TTA***n*-devices. In fact, the power conversion efficiencies of tetrathienoanthracene-based HTMs are comparable to the state-of-

the-art *Spiro*-OMeTAD; in particular, **TTA3**/PSC exhibits a short circuit current density of 22.18 mA/cm^2, a V_{OC} of 1.15 V, and a fill factor of 0.73 yielding 18.76% power conversion efficiency under one sun.

In summary, this work proves **TTA3** as a powerful candidate to substitute *Spiro*-OMeTAD as reference HTM, owing to its facile synthesis and low production costs, its thermal stability, and the high PCE showed in mixed-perovskite devices. Future work is also devoted to prepare perovskite-optimized devices with this outstanding molecule, in the search of higher efficiencies.

4. Experimental Section

4.1. Synthesis and characterization

The detailed synthesis, procedures and characterisation of all compounds are given in Supporting Information.

4.2 Solar Cells Preparation and Characterization

4.2.1. Materials

4-*tert*-butylpyridine (TBP) and bis (trifluoromethylsulfonyl)-imide lithium salt (Li-TFSI) were purchased at Sigma Aldrich, tris(2-(1H-pyrazol-1-yl)-4-*tert*-butylpyridine) cobalt(III) tri[bis(trifluoromethane)sulfonimide] (FK 209; Co(III) TFSI salt) at Dyenamo, lead iodide and lead bromide at TCI, formamidinium iodide, methylammonium bromide, the mesoporous TiO_2 paste (30 NR-D) at Dyesol, and Caesium Iodine at Abcr.

4.2.2. Device preparation

Conductive FTO glass (NSG10) was cleaned by sonication in a 2 % Helmanex solution for 45 min, and then successively washed with water, ethanol and isopropanol. A further UV/O_3 treatment was done for 30 min to remove any traces of residual organic materials prior to the deposition of the functional layers. Next, a 30 nm TiO_2 blocking layer was applied to the

substrates by spray pyrolysis at 450°C from a precursor solution of titanium diisopropoxide bis(acetylacetonate) in anhydrous ethanol. For the mesoporous TiO_2 layer, the TiO_2 paste (30 NR-D) was diluted in ethanol (ratio 1:9 w/w) and then applied to the substrate by spin-coating at 2000 rpm for 10s followed by a sintering step at 500 °C for 20 min. The following steps of the device preparation were done in a glovebox under a nitrogen atmosphere. The perovskite precursor solution was prepared in two steps as follow: a first double-mixed perovskite precursor solution composed of PbI_2 (1.15 M), $PbBr_2$ (0.2 M), formamidinium iodide (1.1 M) and methylammonium bromide (0.2 M) dissolved in a 1:4 mixture of DMSO:DMF was prepared. Then CsI, predissolved as a 1.5 M stock solution in DMSO, was added to the mixed perovskite precursor in a 1:10 ratio (*v*/*v*) to achieve the desired triple cation composition $Cs_{0.1}FA_{0.74}MA_{0.13}PbI_{2.48}Br_{0.39}$. The perovskite solution was spun at 5000 rpm for 30 s using a ramp of 3000 rpm/s. 15 s prior to the end of the spin-coating sequence, 100 µL of chlorobenzene were poured onto the spinning substrate. Afterwards, the substrates were transferred onto a heating plate and annealed at 100 °C for 45 min. The hole-transporting material (**TTA***n* and **TTB***n*) was prepared in a solution of chlorobenzene (PhCl) or 1,1,2,2-tetrachloroethane (TCE) (final concentrations of 10–50 mM, see Table S1 in Supporting Information for details). To this solution, were successively added TBP (3.3 eq/HTM), a 1.8M stock solution of Li-TFSI in AcCN (0.5 eq/HTM), and a 0.25 M stock solution of Co(III)-TFSI in AcCN (0.05 eq/HTM), as additives. The reference HTM solution was prepared at 60 mM of *Spiro*-OMeTAD in TCE, incorporating the same standard composition of additives (see above). The HTM solutions were spin-coated onto the perovskite layers at 4000 rpm for 20 s. Finally, the gold electrodes were deposited by thermal evaporation of 100 nm gold using a shadow mask under high vacuum conditions.

4.2.3. Device characterization

Current-voltage characteristics were measured in air under AM1.5G simulated sunlight with Keithley potentiostat (1 sun; P_{in} = 100mW/cm^2). The light intensity was measured for calibration with an NREL certified KG5 filtered Si reference diode. The solar cells were masked with a metal aperture of 0.16 cm^2 to define the active area. The current-voltage curves were recorded scanning at 10 mVs^{-1} from forward scan to short circuit and *vice versa*, with a preconditioning of the device with light during 3s before the scan.

Supporting Information

Supporting Information is available from the Wiley Online Library or from the author.

Acknowledgements

We are grateful for the financial support of the MINECO, Spain (CTQ2014-52869-P and CTQ2017-85393-P), the Comunidad de Madrid (FOTOCARBON, S2013/MIT-2841). D.A. Meza Rojas thanks the National Council on Science and Technology (CONACYT), No. 239120. M. Urbani thanks Cost Action (COST-STSM-MP1307) within the EU Framework Programme Horizon 2020.

Received: ((will be filled in by the editorial staff))
Revised: ((will be filled in by the editorial staff))
Published online: ((will be filled in by the editorial staff))

References

[1] H. J. Snaith, *J. Phys. Chem. Lett.* **2013**, *4*, 3623.

[2] B. Saparov, D. B. Mitzi, *Chem. Rev.* **2016**, *116*, 4558.

[3] M. Grätzel, *Nat. Mater.* **2014,** *13*, 838.

[4] M. M. Lee, J. Teuscher, T. Miyasaka, T. N. Murakami, H. J. Snaith, *Science* **2012**, *338*, 643.

[5] M. Liu, M. B. Johnston, H. J. Snaith, *Nature* **2013**, *501*, 395.

[6] J. Burschka, N. Pellet, S.-J. Moon, R. Humphry-Baker, P. Gao, M. K. Nazeeruddin, M. Grätzel, *Nature* **2013**, *499*, 316.

[7] J. H. Heo, S. H. Im, J.-H. Noh, T. N. Mandal, C.-S. Lim, J. A. Chang, Y. H. Lee, H.-J. Kim, A. Sarkar, M. K. Nazeeruddin, M. Grätzel, S. I. Seok, *Nat. Photon.* **2013**, *7*, 486.

[8] N. J. Jeon, J. H. Noh, W. S. Yang, Y. C. Kim, S. Ryu, J. Seo, S. I. Seok, *Nature* **2015**, *517*, 476.

[9] M. Saliba, J.-P. Correa-Baena, M. Grätzel, A. Hagfeldt, A. Abate, *Angew. Chem., Int. Ed.* **2018**, 57, 2554; *Angew. Chem.* **2018**, 130, 2582.

[10] V. D'Innocenzo, G. Grancini, M. J. P. Alcocer, A. R. S. Kandada, S. D. Stranks, M. M. Lee, G. Lanzani, H. J. Snaith, A. Petrozza, *Nature Commun.* **2014** , *5*, 3586.

[11] D. Shi, V. Adinolfi, R. Comin, M. Yuan, E. Alarousu, A. Buin, Y. Chen, S. Hoogland, A. Rothenberger, K. Katsiev, Y. Losovyj, X. Zhang, P. A. Dowben, O. F. Mohammed, E. H. Sargent, O. M. Bakr, *Science* **2015**, *347*, 519.

[12] Q. Dong, Y. Fang, Y. Shao, P. Mulligan, J. Qiu, L. Cao, J. Huang, *Science* **2015**, *347*, 967.

[13] J. H. Noh, S. H. Im, J. H. Heo, T. N. Mandal, S. I. Seok, *Nano Lett.* **2013**, *13*, 1764.

[14] M. M. Lee, J. Teuscher, T. Miyasaka, T. N. Murakami, H. J. Snaith, *Science* **2012**, *338*, 643.

[15] B. Conings, J. Drijkoningen, N. Gauquelin, A. Babayigit, J. D'Haen, L. D'Olieslaeger, A. Ethirajan, J. Verbeeck, J. Manca, E. Mosconi, F. D. Angelis, H.-G. Boyen, *Adv. Energy Mater.* **2015**, *5*, 1500477.

[16] R. K. Misra, S. Aharon, B. Li, D. Mogilyansky, I. Visoly-Fisher, L. Etgar, E. A. Katz, *J. Phys. Chem. Lett.* **2015**, *6*, 326.

[17] G. Niu, X. Guo, L. Wang, *J. Mater. Chem. A* **2015**, 3, 8970.

[18] N. Aristidou, C. Eames, I. Sanchez-Molina, X. Bu, J. Kosco, M. S. Islam, S. A. Haque, *Nature Commun.* **2017**, *8*, 15218.

[19] J.-W. Xiao, L. Liu, D. Zhang, N. De Marco, J.-W. Lee, O. Lin, Q. Chen, Y. Yang, *Adv. Energy Mater.* **2017**, *7*, 1700491.

[20] S. Yang, W. Fu, Z. Zhang, H. Chen, C.-Z. Li, *J. Mater. Chem. A* **2017**, *5*, 11462-11482.

[21] A. Sadhanala, F. Deschler, T. H. Thomas, S. n. E. Dutton, K. C. Goedel, F. C. Hanusch, M. L. Lai, U. Steiner, T. Bein, P. Docampo, D. Cahen, R. H. Friend, *J. Phys. Chem. Lett.* **2014**, *5*, 2501-2505.

[22] G. E. Eperon, S. D. Stranks, C. Menelaou, M. B. Johnston, L. M. Herz, H. J. Snaith, *Energy Environ. Sci.* **2014**, 7, 982.

[23] M. Saliba, T. Matsui, J.-Y. Seo, K. Domanski, J.-P. Correa-Baena, M. K. Nazeeruddin, S. M. Zakeeruddin, W. Tress, A. Abate, A. Hagfeldt, M. Grätzel, *Energy Environ. Sci.* **2016**, *9*, 1989.

[24] H. Tan, A. Jain, O. Voznyy, X. Lan, F. P. García de Arquer, J. Z. Fan, R. Quintero-Bermudez, M. Yuan, B. Zhang, Y. Zhao, F. Fan, P. Li, L. N. Quan, Y. Zhao, Z.-H. Lu, Z. Yang, S. Hoogland, E. H. Sargent, *Science* **2017**, *355*, 722.

[25] K. T. Cho, G. Grancini, Y. Lee, E. Oveisi, J. Ryu, O. Almora, M. Tschumi, P. A. Schouwink, G. Seo, S. Heo, J. Park, J. Jang, S. Paek, G. Garcia-Belmonte, M. K. Nazeeruddin, *Energy Environ. Sci.* **2018**, *11*, 952.

[26] C. Hu, Y. Bai, S. Xiao, T. Zhang, X. Meng, W. K. Ng, Y. Yang, K. S. Wong, H. Chen, S. Yang, *J. Mater. Chem. A* **2017**, *5*, 21858.

[27] G. Grancini, C. Roldán-Carmona, I. Zimmermann, E. Mosconi, X. Lee, D. Martineau, S. Narbey, F. Oswald, F. De Angelis, M. Grätzel, M. K. Nazeeruddin, *Nature Commun.* **2017**, *8*, 15684.

[28] Z. Fan, K. Sun, J. Wang, *J. Mater. Chem. A* **2015**, *3*, 18809.

[29] L. Z. Tan, F. Zheng, S. M. Young, F. Wang, S. Liu, A. M. Rappe, *Npj Comput. Mater.* **2015**, *2*, 16026.

[30] F. Zheng, H. Takenaka, F. Wang, N. Z. Koocher, A. M. Rappe, *J. Phys. Chem. Lett.* **2015**, *6*, 31.

[31] Y. Li, M. Behtash, J. Wong, K. Yang, *J. Phys. Chem. C* **2018**, *122*, 177.

[32] H.-Y. Ye, W.-Q. Liao, C.-L. Hu, Y. Zhang, Y.-M. You, J.-G. Mao, P.-F. Li, R.-G. Xiong, *Adv. Mater.* **2016**, *28*, 2579.

[33] W.-Q. Liao, Y. Zhang, C.-L. Hu, J.-G. Mao, H.-Y. Ye, P.-F. Li, S. D. Huang, R.-G. Xiong, *Nature Commun.* **2015**, *6*, 7338.

[34] J. Burschka, A. Dualeh, F. Kessler, E. Barano, N.-L. Cevry-Ha, M. K. Nazeeruddin, M. Gratzel, *J. Am. Chem. Soc.* **2011**, *133*, 18042.

[35] L. Calil, S. Kazim, M. Grätzel, S. Ahmad, *Angew. Chem. Int. Ed.* **2016**, *55*, 14522.

[36] P. Agarwala, D. Kabra, *J. Mater. Chem. A* **2017**, *5*, 1348.

[37] S. Park, J. H. Heo, J. H. Yun, T. S. Jung, K. Kwak, M. J. Ko, C. H. Cheon, J. Y. Kim, S. H. Im, H. J. Son, *Chem. Sci.* **2016**, *7*, 5517.

[38] X. Jiang, K. M. Karlsson, E. Gabrielsson, E. M. J. Johansson, M. Quintana, M. Karlsson, L. Sun, G. Boschloo, A. Hagfeldt, *Adv. Funct. Mater.* **2011**, *21*, 2944.

[39] B. Xu, E. Sheibani, P. Liu, J. Zhang, H. Tian, N. Vlachopoulos, G. Boschloo, L. Kloo, A. Hagfeldt, L. Sun, *Adv. Mat.* **2014**, *26*, 6629.

[40] H. Li, K. Fu, P. P. Boix, L. H. Wong, A. Hagfeldt, M. Grätzel, S. G. Mhaisalkar, A. C. Grimsdale, *ChemSusChem* **2014**, *7*, 3420.

[41] H. Li, K. Fu, A. Hagfeldt, M. Grätzel, S. G. Mhaisalkar, A. C. Grimsdale, *Angew. Chem. Int. Ed.* **2014**, *53*, 4085.

[42] M. L. Petrus, T. Bein, T. J. Dingemans, P. Docampo, *J. Mater. Chem. A* **2015**, *3*, 12159.

[43] H. Wang, A. D. Sheikh, Q. Feng, F. Li, Y. Chen, W. Yu, E. Alarousu, C. Ma, M. A. Haque, D. Shi et al., *ACS Photonics* **2015**, *2*, 849.

[44] N. J. Jeon, J. Lee, J. H. Noh, M. K. Nazeeruddin, M. Grätzel, S. I. Seok, *J. Am. Chem. Soc.* **2013**, *135*, 19087.

[45] A. Molina-Ontoria, I. Zimmermann, I. García-Benito, P. Gratia, C. Roldán-Carmona, S. Aghazada, M. Grätzel, M. K. Nazeeruddin, N. Martín, *Angew. Chem. Int. Ed.* **2016**, *55*, 6270.

[46] A. Abate, S. Paek, F. Giordano, J.-P. Correa-Baena, M. Saliba, P. Gao, T. Matsui, J. Ko, S. M. Zakeeruddin, K. H. Dahmen, A. Hagfeldt, M. Grätzel, M. K. Nazeeruddin, *Energy Environ. Sci.* **2015**, *8*, 2946.

[47] M. Franckevicius, A. Mishra, F. Kreuzer, J. Luo, S. M. Zakeeruddin, M. Grätzel, *Mater. Horiz.* **2015**, *2*, 613.

[48] M. Saliba, S. Orlandi, T. Matsui, S. Aghazada, M. Cavazzini, J.-P. Correa-Baena, P. Gao, R. Scopelliti, E. Mosconi, K.-H. Dahmen, F. De Angelis, A. Abate, A. Hagfeldt, G. Pozzi, M. Grätzel, M. K. Nazeeruddin, *Nat. Energy* **2016**, *1*, 15017.

[49] I. Zimmermann, J. Urieta-Mora, P. Gratia, J. Aragó, G. Grancini, A. Molina-Ontoria, E. Ortí, N. Martín, M. K. Nazeeruddin, *Adv. Energy. Mater.* **2016**, 16011674.

[50] J. L. Brusso, O. D. Hirst, A. Dadvand, S. Ganesan, F. Cicoira, C. M. Robertson, R. T. Oakley, F. Rosei, D. F. Perepichka, *Chem. Mater.* **2008**, *20*, 2484.

[51] K. Do, H. Choi, K. Lim, H. Jo, J. W. Cho, M. K. Nazeeruddin, J. Ko, *Chem. Commun.* **2014**, *50*, 10971.

[52] D. Lumpi, B. Holzer, J. Bintinger, E. Horkel, S. Waid, H. D. Wanzenbock, M. Marchetti-Deschmann, C. Hametner, E. Bertagnolli, I. Kymissis, J. Frohlich, *New J. Chem.* **2015**, *39*, 1840.

[53] M. L. Petrus, T. Bein, T. J. Dingemans, P. Docampo, J. Mater. Chem. A, **2015**, *3*, 2159.

[54] Z. He, C.-W. Kan, C.-L. Ho, W.-Y. Wong, C.-H. Chui, K.-L. Tong, S.-K. So, T.-H. Lee, L. M. Leung, Z. Lin, *Dyes Pigm.* **2011**, *88*, 333.

[55] C. M. Cardona, W. Li, A. E. Kaifer, D. Stockdale, G. C. Bazan, *Adv. Mat.* **2011**, *23*, 2367.

[56] J.-L. Bredas, *Mater. Horiz.* **2014**, *1*, 17.

[57] K. T. Cho, O. Trukhina, C. Roldán-Carmona, M. Ince, P. Gratia, G. Grancini, P. Gao, T. Marszalek, W. Pisula, P. Y. Reddy, T. Torres, M. K. Nazeeruddin, *Adv. Energy Mater.* **2017**, *7*, 1601733.

[58] H.-S. Kim, C.-R. Lee, J.-H. Im, K.-B. Lee, T. Moehl, A. Marchioro, S.-J. Moon, R. Humphry-Baker, J.-H. Yum, J. E. Moser, M. Grätzel, N.-G. Park, *Sci. Reports* **2012**, *2*, 591.

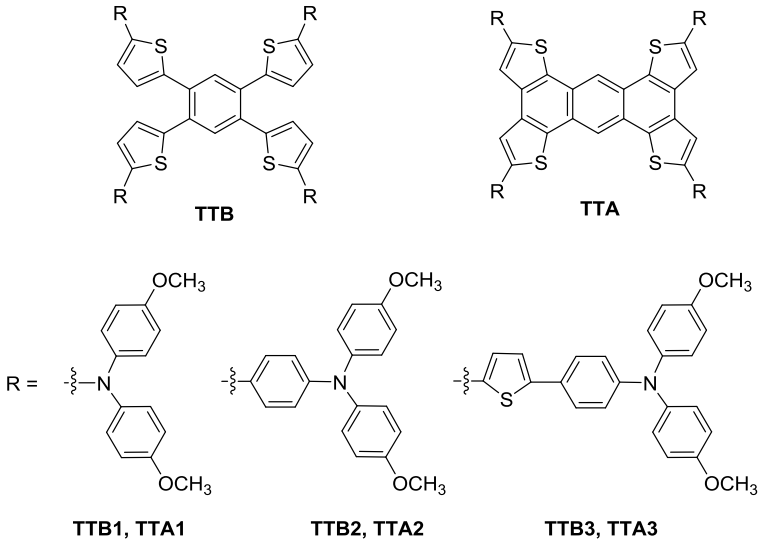

Figure 1. Structure of **TTB***n* and **TTA***n* synthesized in this work.

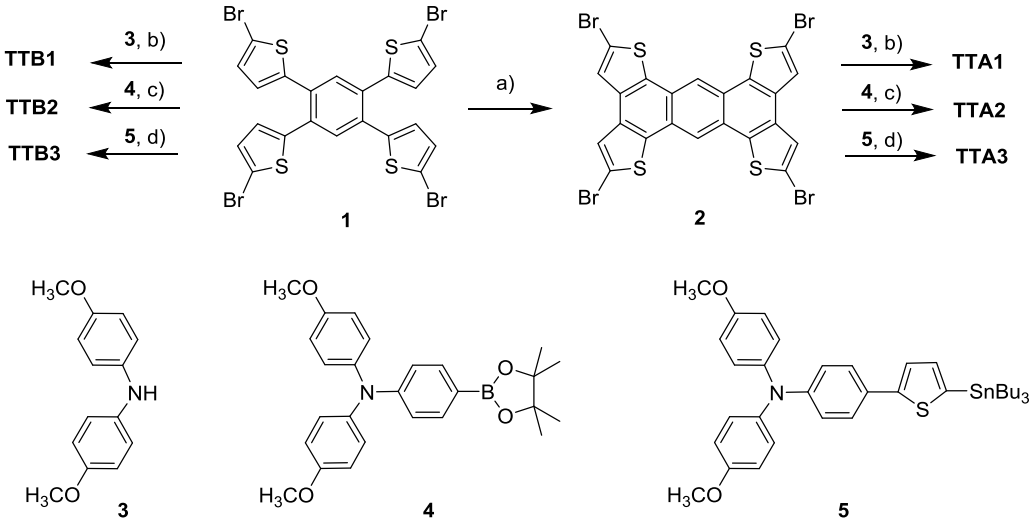

Scheme 1. Synthesis of **TTB1**-**3** and **TTA1**-**3**. Reagents and conditions: a) $FeCl_3$, $MeNO_2$/PhCl, 60°C, 1h, (93%); b) $Pd_2(dba)_3$, Xphos, ^{t}BuONa, toluene, 100 °C, 4 days (**TTB1**: 35%; **TTA1**: 32%). c) K_3PO_4, $Pd(PPh_3)_4$, DMF, 100 °C, 4 days (**TTB2**: 55%; **TTA2**: 70%); d) $Pd(PPh_3)_4$, toluene , 4 days, 100 °C (**TTB3**:40 %; **TTA3**: 85%).

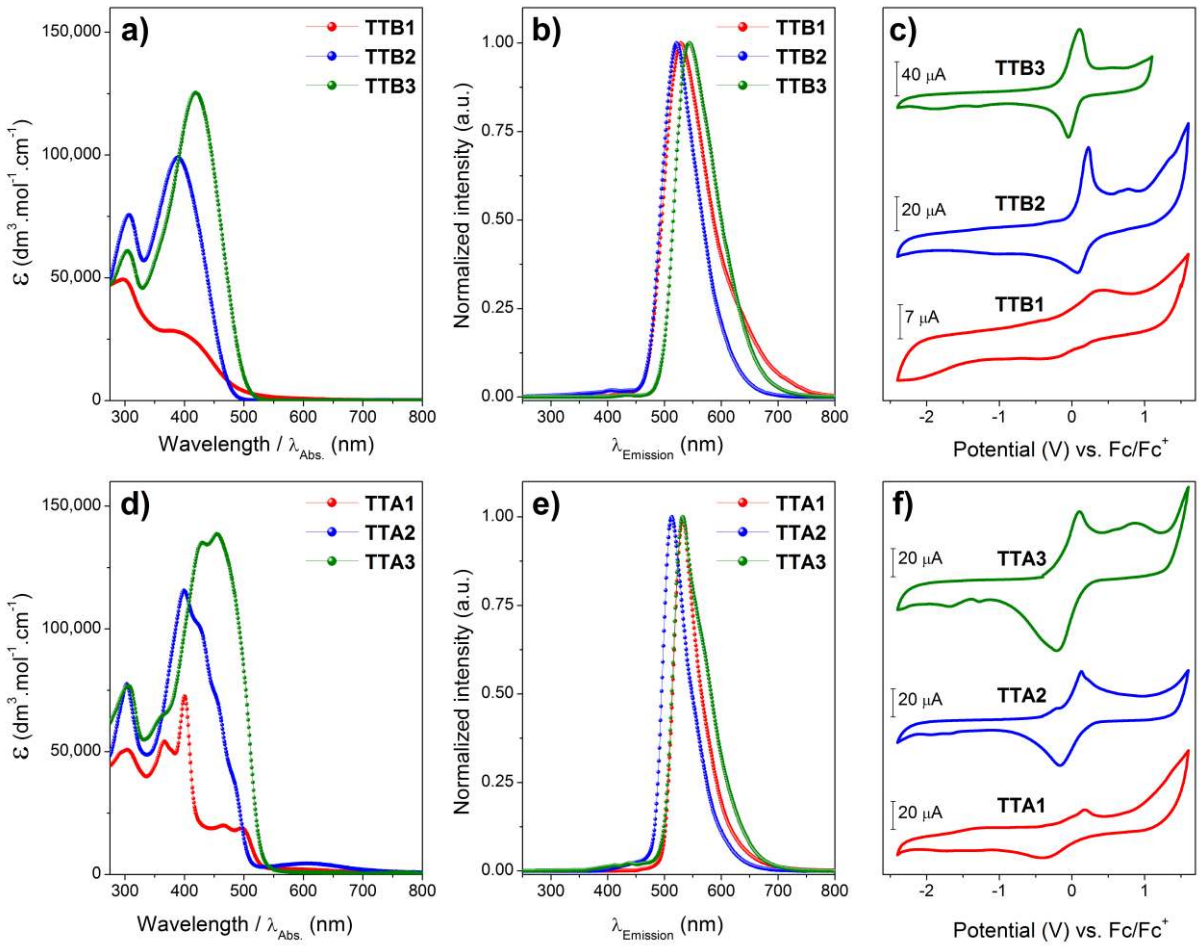

Figure 2. UV-Vis absorption (a) and normalized emission (b) spectra of **TTB1-3** in $CHCl_3$ solutions (for emission spectra, excitation was done at λ_{max} of absorption between 385 nm and 419 nm; see Table 1). c) Cyclic voltammograms (Scan rate 0.1 V/s) of **TTB1-3**, as drop-casted films deposited on a platinum electrode, and recorded in 0.1 M tetrabutylammonium hexafluorophospate solutions in acetonitrile.; reference electrode: $Ag/AgNO_3$; calibrated with (Fc/Fc^+) as an external reference. Normalized UV-absorption (d) and emission (e) (excitation at λ_{max} of absorption) spectra of **TTA1-3** in $CHCl_3$. f) Cyclic voltammograms (Scan rate 0.1 V/s) of **TTA1-3**, as drop-casted films deposited on a platinum electrode, and recorded in 0.1 M tetrabutylammonium hexafluorophospate solutions in acetonitrile; reference electrode: $Ag/AgNO_3$; calibrated with (Fc/Fc^+) as an external reference.

Table 1. Electrochemical and optical properties of **TTB***n* and **TTA***n* derivatives

HTM	$\lambda_{max,\ abs\ (log\ \varepsilon)}$ [nm]	$\lambda_{max,\ em}$ [nm]	$E_{0\text{-}0}$ [a] [eV]	$E_{ox}^{1/2}$ [V] *vs.* Fc/Fc$^+$	E_{HOMO} [b] [eV]	E_{LUMO} [c] [eV]
TTB1	297 (4.69) 385 (br sh, 4.45)	528	2.59	0.38	-5.48	-2.89
TTB2	307 (4.88) 389 (5.10)	521	2.64	0.22	-5.32	-2.68
TTB3	304 (4.78) 419 (5.10)	541	2.50	0.10	-5.20	-2.70
TTA1	304 (4.71) 366 (4.73) 400 (4.86) 465 (4.30) 496 (4.28)	532	2.46	0.17	-5.27	-2.81
TTA2	303 (4.89) 399 (5.06) 608 (3.56)	513	2.55	0.13	-5.23	-2.68
TTA3	306 (4.89) 357 (br sh, 4.80) 430 (5.13) 455 (5.13)	532	2.44	0.10	-5.20	-2.76

[a] $E_{0\text{-}0}$ is the zero-zero excitation energy obtained from the intersection between the normalized absorption and emission spectra.; [b] E_{HOMO} was calc. as $E_{HOMO} = -(E_{[onset,\ ox\ vs.\ Fc/Fc+]} + 5.1)$ (eV); [c] E_{LUMO} was calc. as $E_{HOMO} + E_{0\text{-}0}$.

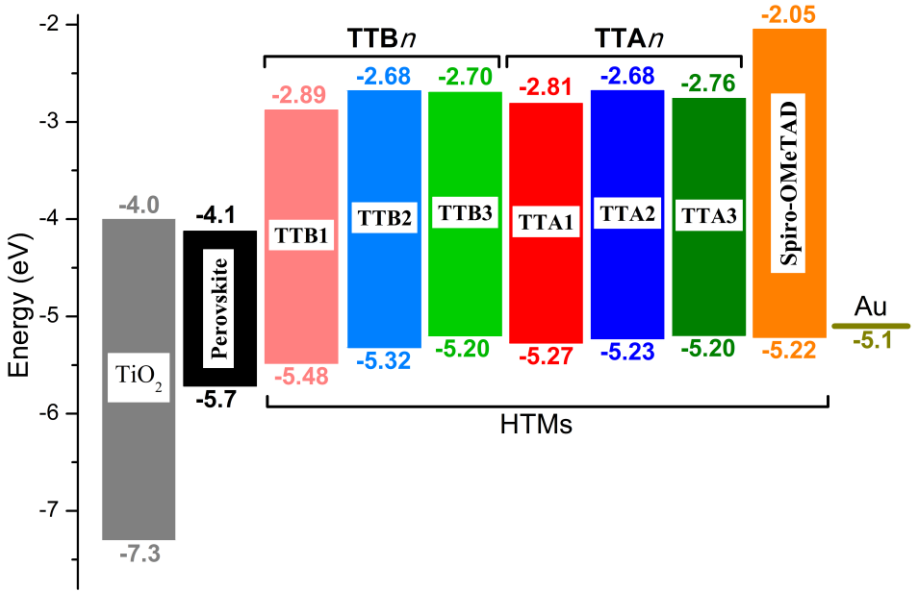

Figure 3. Schematic representation of the energy levels of **TTB***n*, **TTA***n* and *Spiro*-OMeTAD HTMs in comparison with the band energies of TiO_2, mixed-perovskite and the Au electrode (values of TiO_2, Au electrode and *Spiro*-OMeTAD are taken from ref [57] and those of mixed-perovskite from ref [26]).

Table 2. Device performances made with the HTMs **TTB***n* and **TTA***n* compared to *Spiro*-OMeTAD under simulated 1 sun illumination (P_{in} = 100mW/cm^2; AM1.5G standard conditions).

HTM[a]	V_{OC} [V]	J_{SC} [mA/cm^2]	F.F. [%]	PCE [%]
Spiro-OMeTAD	1.097	22.59	75.8	18.77
TTB1	0.843	4.11	61.6	2.13
TTB2	0.972	8.67	72.7	6.12
TTB3	0.975	10.92	66.0	7.03
TTA1	1.025	20.16	80.1	16.54
TTA2	0.754	21.21	60.5	9.69
TTA2[b]	0.994	22.68	62.5	14.09
TTA3	1.153	22.18	73.3	18.76

[a] Excepted otherwise noted, HTMs were spin-coated from 1,1,2,2-tetrachloroethane solutions. [b] **TTA2** spin-coated from PhCl solution.

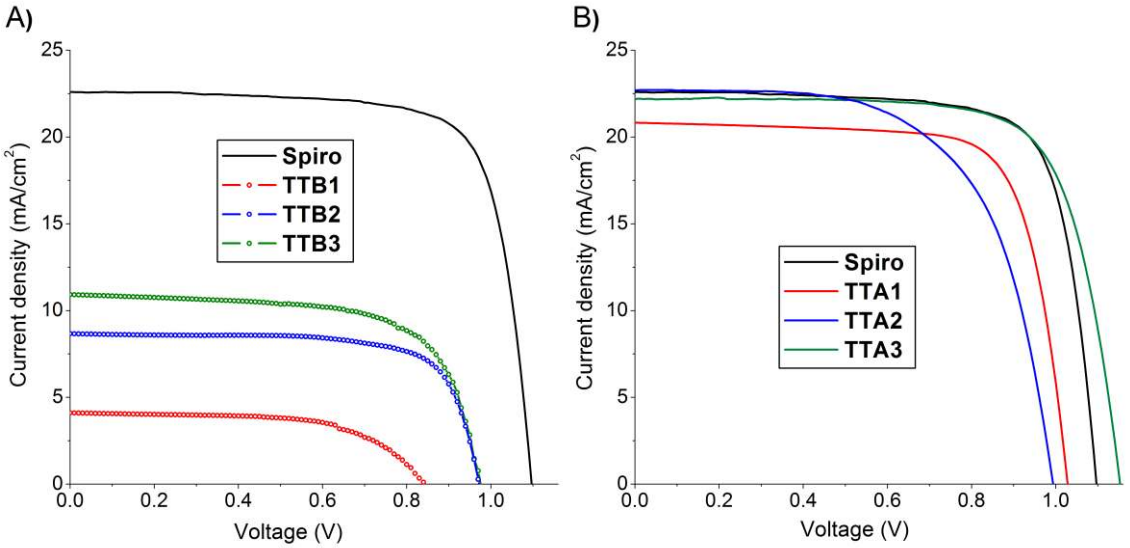

Figure 4. *J/V* curves of the best perovskite solar cells using A) **TTB***n* and B) **TTA***n* as HTMs under simulated one sun illumination (P_{in} = 100mW/cm^2; AM1.5G standard conditions). *J/V* curve of the reference cell made with the standard *Spiro*-OMeTAD as HTM is depicted for comparison. All HTMs were spin-coated from TCE solutions except **TTA2** from PhCl (See Table 2).

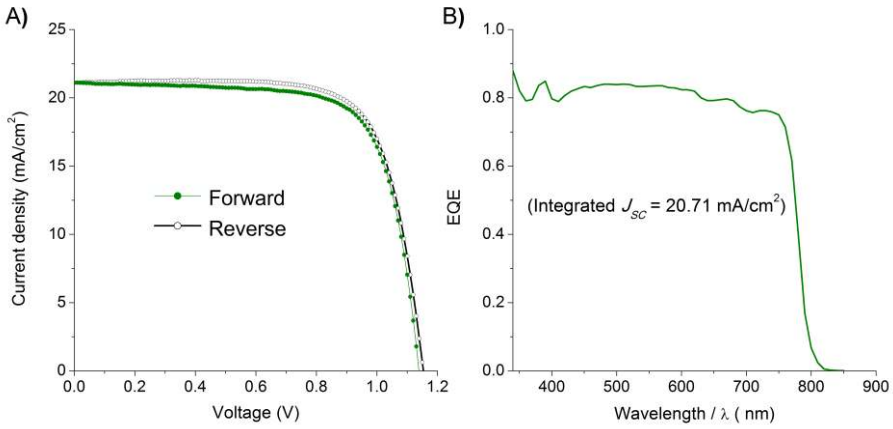

Figure 5. A) *J/V* curve under forward and reverse bias (scan rate 10 mV s^{-1}) and B) EQE as a function of wavelength, measured for one of the best PSC cell made with HTM **TTA3**.

Table 3. Hysteresis characteristics of **TTA3**/PSC device under forward and reverse bias, corresponding to the *J/V* curves presented in Figure 5A.[(a)]

Bias	V_{OC} [V]	J_{SC} [mA/cm^2]	F.F. [%]	PCE [%]
Forward	1.153	21.09	73.5	17.89
Reverse	1.138	21.11	72.6	17.44

[(a)] Scan rate of 10 mV s^{-1}

Table of contents entry

Two related families of star-shaped thiophene-containing small molecules based on fused tetrathienoanthracene (TTAn) and non-fused tetrathienylbenzene (TTBn) cores are tested as hole transporting materials (HTMs) in mixed-ion perovskite solar cells (PSCs). The best tested HTM, TTA3, reached similar power conversion efficiency in PSC than the standard *Spiro*-OMeTAD, with maxima PCE of 18.8% under simulated one sun illumination (AM1.5G).

Keyword solar energy conversion – perovskite solar cells – hole-transporting materials – tetrathienoanthracenes – tetrathienylbenzenes

Diana Elizabeth Meza Rojas, Kyung Taek Cho, Yi Zhang, Maxence Urbani, Nouar Tabet, Gema de la Torre, Mohammad Khaja Nazeeruddin,* Tomás Torres **

Tetrathienoanthracene and Tetrathienylbenzene Derivatives as Hole-Transporting Materials for Perovskite Solar Cell